Experiments using new initial soil moisture conditions and soil map in the Eta model over La Plata Basin

Moira E. Doyle, Javier Tomasella, Daniel A. Rodriguez & Sin Chan Chou

Meteorology and Atmospheric Physics

ISSN 0177-7971
Volume 121
Combined 3-4

Meteorol Atmos Phys (2013)
121:119-136
DOI 10.1007/s00703-013-0265-5

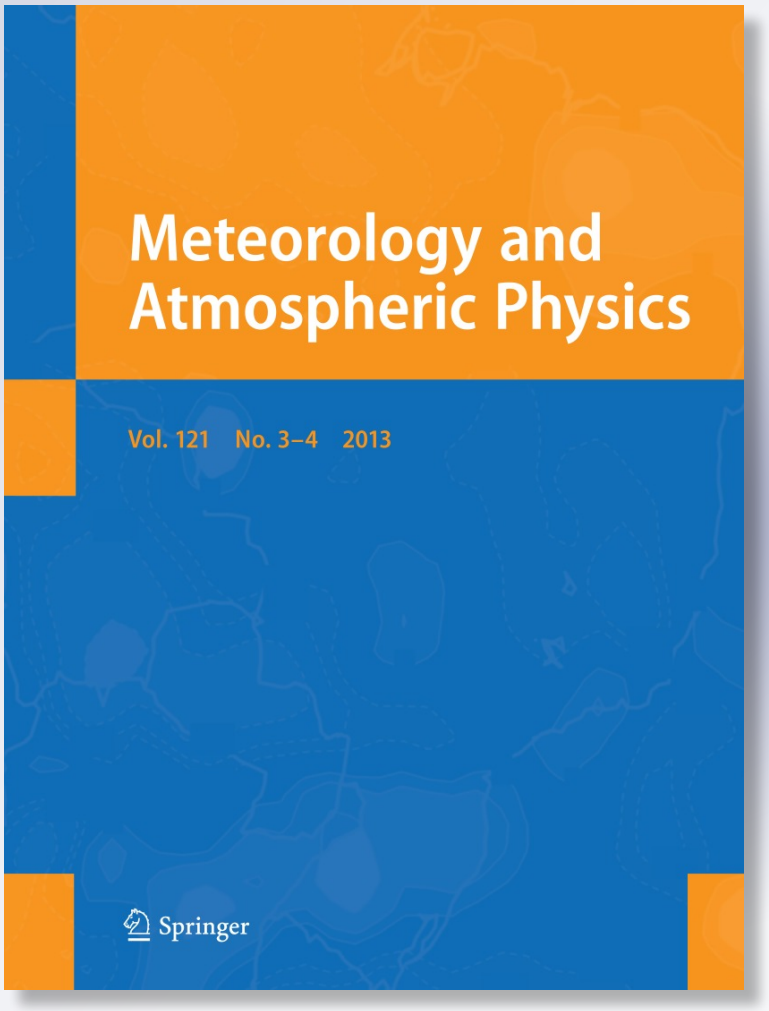

Springer

Meteorol Atmos Phys (2013) 121:119–136
DOI 10.1007/s00703-013-0265-5

ORIGINAL PAPER

Experiments using new initial soil moisture conditions and soil map in the Eta model over La Plata Basin

Moira E. Doyle · Javier Tomasella · Daniel A. Rodriguez · Sin Chan Chou

Received: 21 October 2011 / Accepted: 15 May 2013 / Published online: 31 May 2013

Abstract An effort towards a more accurate representation of soil moisture and its impact on the modeling of weather systems is presented. Sensitivity tests of precipitation to soil type and soil moisture changes are carried out using the atmospheric Eta model for the numerical simulation of the development of a mesoscale convective system over northern Argentina. Modified initial soil moisture conditions were obtained from a hydrological balance model developed and running operationally at INPE. A new soil map was elaborated using the available soil profile information from Brazil, Paraguay, Uruguay, and Argentina and depicts 18 different soil types. Results indicate that more accurate initial soil moisture conditions and incorporating a new soil map with hydraulic parameters, more representative of South American soils, improve daily total precipitation forecasts both in quantitative and spatial representations.

Responsible editor: F. Mesinger.

M. E. Doyle (✉)
Centro de Investigaciones del Mar y la Atmosfera (CIMA/CONICET-UBA)-UMI IFAECI/CNRS, Buenos Aires, Argentina
e-mail: doyle@cima.fcen.uba.ar

M. E. Doyle
Departamento de Ciencias de la Atmósfera y los Océanos, FCEyN, Univ. Buenos Aires, Buenos Aires, Argentina

J. Tomasella · D. A. Rodriguez · S. C. Chou
Instituto Nacional de Pesquisas Espaciais, Centro de Ciência do Sistema Terrestre (CCST–INPE, Brazil), São paulo, Brazil

Present Address:
J. Tomasella
Centro Nacional de Monitoramento e Alertas de Desastres Naturais (CEMADEN, Brazil), São paulo, Brazil

1 Introduction

Soil moisture initial conditions in regional models are sometimes based on simulations of global atmospheric models with low spatial resolution which have been initialized with global data sets of soil moisture (e.g. Mintz and Serafini 1992; Schemm et al. 1992; Liston et al. 1993). These simulations are forced with monthly average or daily temperature and precipitation observations. There are large discrepancies between these values and observations, particularly in the tropics, due to limitations in the parameterization of hydrological processes, which dampens soil moisture interannual variability (Robock et al. 2000). However, the latest generation of numerical weather prediction models aims to accurately predict soil moisture.

Based on observations, Entekhabi et al. (1996) showed that the strong interactions between soil moisture and the atmospheric processes take place in all spatial and temporal scales. Reen et al. (2006) investigated the potential benefits on simulated atmospheric boundary layer structure of a better specification of soil moisture and related parameters within a mesoscale model with different land-surface physics options. During the Southern Great Plains Hydrology Experiment in 1997 an L-band passive microwave radiometer was flown on a P-3 aircraft and used to derive surface (0–50 mm) soil moisture (Jackson et al. 1995, 1999). The authors showed that the addition of more detailed soil moisture produced noticeable improvements in the model's representation of surface air temperature and mixing ratio gradients.

Soil moisture interacts with the overlaying atmosphere through surface energy and water balances, and the amount of soil moisture strongly influences the degree of heat and moisture exchange between the land and the atmosphere

(Qu et al. 1998; Dirmeyer et al. 2000; Zhu and Liang 2005). As pointed out by Dirmeyer et al. (1999), soil moisture also determines the partitioning of land surface heat flux between sensible and latent components, thus affecting both heat and water balances. The soil moisture also influences the conditions of the overlaying vegetation through transpiration and radiative properties. An increase in soil moisture damps any increase in land surface temperature caused by solar radiation; on the other hand, increase in soil moisture may lead to increase in evaporation, which in turn strongly influences atmospheric convection and precipitation. The release of latent heat associated with the cumulus convection enhances low-level moisture convergence and thus further intensifies precipitation (Lau and Bua 1998).

Entekhabi and Brubaker (1995), Brubaker and Entekhabi (1996) also performed an in-depth quantitative analysis of land–atmosphere interactions that focused on the impacts of near-surface soil moisture and temperature variability on fluxes and planetary boundary layer (PBL) evolution. They found evidence that PBL growth can enhance surface sensible heat flux through a complex set of processes that lead to rapid soil drying and, hence, higher surface Bowen ratio (Kim and Entekhabi 1998). Santanello et al. (2007) further examined the interactions that determine PBL evolution and land surface energy balance, in particular, the relationships among land surface properties and fluxes, the PBL structure, atmospheric stability, and soil moisture. Their results showed that the first-order effects of land–atmosphere coupling are manifested in the control of soil moisture and stability on atmospheric demand for evapotranspiration and on the surface energy balance. Moreover, day-to-day changes in the spatial variability of soil moisture can have significant impact on the surface energy budget, on the convective available potential energy, and on the convective inhibition. Differential heating due to horizontal gradients in the soil moisture may be important in the convective development (Gallus and Segal 2000; Chang and Wetzel 1991).

Pielke (2001) showed that the effects of soil moisture on rainfall can be associated with dynamical modifications of atmospheric systems as well as the generation of mesoscale circulations through the formation of spatial sensible heat flux gradients. Analyses of convective events have shown that surface moisture can influence cloud formation (Ek and Holtslag 2004), the evolution of the convection and precipitation. Lanicci et al. (1987) showed that variability in soil moisture conditions is important for generating differential surface heating and low-level thermodynamic instability through strong surface evaporation.

Sutton et al. (2006) showed that warm season rainfall forecasts are dependent on the soil moisture initial condition uncertainty. Following this idea Aligo et al. (2007) analyzed the summer rainfall forecast spread in weakly forced and strongly forced events from an ensemble with different soil moisture analyses. They concluded that the precipitation amount within convective systems can be strongly sensitive to soil moisture perturbations, but the perturbations, if only applied to soil moisture, might not add enough variability to rainfall forecasts over the entire domain.

Soil moisture can have a noticeable impact upon situations with stronger forcing such as frontal passages (Fast and McCorcle 1991). Koch et al. (1997) found that a reduction of soil wetness in the warm sector ahead of a cold front increased the precipitation due to a corresponding intensification of the frontal dynamic effects (i.e., convergence). According to Gallus and Segal (2000) modification of soil moisture has the following impacts on cold fronts accompanied by convection: (1) increasing soil moisture causes evapotranspiration to enhance thermodynamically the potential convection, (2) persisting cloud cover in the cold sector behind the front intensifies the cross-front temperature gradient as the soil in the warm frontal sector becomes drier (Segal et al. 1993) and (3) increasing soil moisture results in a less developed convective boundary layer and reduced cross-isobaric flow.

Employing the NCEP Eta Regional Climate Model, Yang et al. (2007) investigated the response of the model's seasonal simulations of summer precipitation to high-frequency variability of soil moisture. They focused on the response of model precipitation and temperature over the U.S. Midwest and Southeast due to imposed changes in the diurnal and synoptic variability of soil moisture during the warm and dry summer of 1988 and a summer with devastating floods of 1993. Their results showed that high-frequency variability of soil moisture increased the precipitation in 1988 but decreased the precipitation in 1993, with major signals in the southern Midwest and the Southeast. Moreover, diurnal variability and synoptic variability of soil moisture caused similar changes in precipitation, indicating the importance of including the diurnal cycle of land surface process in climate modeling.

By analyzing a dozen of AGCM highly controlled numerical experiments, Koster et al. (2004) highlighted hot spots where precipitation and soil moisture anomalies were highly coupled. Notably, they have identified locations where precipitation prediction skills during NH summer could be enhanced by soil moisture initialization.

Temporal and spatial representation of soil moisture in atmospheric models is an issue of constant study since numerical weather prediction models and climate models require an accurate representation of initial land surface conditions to partition properly the sensible and latent

heat fluxes. Furthermore, the determination of soil moisture at each grid point is highly dependent of the soil profile and the hydrologic parameters corresponding to each soil type. Most numerical weather prediction models employ global scale soil classifications grouping in a few categories all the different world-wide soil types and fail to correctly represent the spatial variability of soil types at smaller scales.

In this paper an effort towards a more accurate representation of soil moisture and its impact on the modeling of weather systems is presented. The Eta model is chosen to perform numerical simulations over South America and to test the sensitivity of precipitation to soil and soil moisture changes. The meteorological situation analyzed is a cold front crossing southeastern South America which is followed by the development of a mesoscale convective system over northern Argentina in October 2006.

The structure of the paper is as follows: initial soil moisture conditions are estimated through a hydrological balance model, which is described in Sect. 2; the new soil map derived for the eastern sector of South America covering Brazil, Paraguay, Uruguay, and Argentina north of 40°S is discussed in Sect. 3. The Eta model and the experiments performed are presented in Sect. 4, while the synoptic situation is described in Sect. 5. Results are shown in Sect. 6 and the main conclusions are discussed in Sect. 7.

2 Soil hydrological balance model

Initial soil moisture conditions for the Eta simulations were obtained from a hydrological balance model developed and running operationally at INPE. The model uses integrated daily precipitation (P) derived from TRMM product 3B42 version 6 (http://daac.gsfc.nasa.gov/precipitation/TRMM_README/TRMM_3B42_readme.shtml) on a $0.25° \times 0.25°$ grid, and rain gauge observed precipitation collected by different institutions in Brazil and by the National Weather Services of Argentina, Uruguay, and Paraguay (Rozante et al. 2010).

Time variation of soil water storage above wilting point, S (mm), is estimated using the balance equation (1):

$$\frac{\partial S}{\partial t} = P = \mathrm{RET} - \mathrm{DD} \tag{1}$$

where P indicates the rainfall rate (mm/day), RET actual evapotranspiration (mm/day), and DD the deep drainage rate (mm/day).

Actual evapotranspiration (RET) is linearly derived from the potential evapotranspiration (PET), soil water storage above permanent wilting point (S), and a critical moisture content (CMC) as described by Eq. (2):

$$\begin{aligned} \mathrm{RET} &= \frac{S}{\mathrm{CMC}}\mathrm{PET} \quad S < \mathrm{CMC} \\ \mathrm{RET} &= \mathrm{PET} \quad S \geq \mathrm{CMC} \end{aligned} \tag{2}$$

CMC is a soil parameter that defines the soil water storage threshold above which plant roots can take soil water without stress. This parameter is defined through soil characteristic curves as the amount of water at a −60 kPa matrix potential.

The deep drainage rate is calculated assuming gravity drainage according to

$$\mathrm{DD} = K_s \left(\frac{S}{S_{\max}}\right)^{\eta} \tag{3}$$

where K_s is the saturated soil hydraulic conductivity, $S_{\max}$ the maximum soil moisture content, and η is Brooks–Corey parameter.

By adding both variations the total soil moisture content variation is obtained. When the resulting storage is greater than the maximum soil moisture content ($S_{\max}$), the model considers this an excess (EXCsat) and sets the soil moisture content equal to the maximum soil moisture content (Eq. 4).

$$\begin{aligned} S > S_{\max} &\Rightarrow \mathrm{EXCsat} = S - S_{\max} \\ S &= S_{\max} \end{aligned} \tag{4}$$

The resultant soil moisture fields correspond to values above the wilting point.

3 Soil map

One of the weaknesses of numerical models is their low precipitation forecast skill which is highly dependent on the correct parameterization of the different processes including soil moisture balance. One of the crucial components of this balance is the soil type as it determines important parameters such as wilting point and field capacity (e.g. Wilson et al. 1987). In order to explore to what degree the development of weather systems is determined by accurate soil type definition, a new soil map was developed to replace the existing Eta soil map.

The new soil map was elaborated using the available soil profile information in the INPE soil data base. It includes information on soil profiles from Brazil, Paraguay, Uruguay, and Argentina. Each profile includes basic information such as soil types, texture classes, horizon depths, amount of organic carbon, etc. The different hydrological parameters defining each soil were obtained applying pedotransfer functions (Tomasella and Hodnett 2005).

Soil properties in the Eta model are defined by different parameters including soil quartz content (QTZ), wilting

Table 1 Thresholds used to establish soil types of the new soil map

	I	II	III
Θ_c (mm)	≤75	75–150	>150
Θ_s (mm)	≤200	200–350	>350
Θ_w (mm)	≤150	150–250	>250

point soil moisture contents (Θ_w), saturated soil diffusivity (D), saturated soil hydraulic conductivity (K_s), saturated soil potential (Ψ_s), reference soil moisture for the onset of soil moisture stress in transpiration (Θ_c), maximum soil moisture content (Θ_s), diffusivity/conductivity rate (F), air dry soil moisture content limits (Θ_D), and the B parameter for each soil type (B).

The criterion adopted to delimit the groups and classify the soil data base was, in first place, to select three hydrologic parameters: Θ_c, Θ_s. and Θ_w. For each of these variables, three thresholds were defined (Table 1).

The combination of these three variables and three categories would result in 27 different soil types. However, in some cases no soil from the data base met the requirements; in other cases the group was composed of only a few profiles and in these cases it was decided to include them in similar class. The new soil classification, from the 27 potential types was reduced to 18 soil types identified over the area. The necessary soil and hydrologic Eta parameters were recalculated using the information in the soil data base. In particular, those parameters that were used in the INPE soil hydrological balance model as well as in the Eta land-surface model were taken from the former and converted to match the Eta land-surface unit system. Values of soil and hydrologic parameters are presented in Table 2. However, the vertical structure of the Eta land-surface model is kept unchanged.

Figure 1 presents the area where the new soil map was defined based on the INPE soil data base and gridded onto 0.25° mesh. The area extending over Brazil, Paraguay, Uruguay, and Argentina north of 40°S was covered by the data base; the rest of the continent was completed using the FAO (2007) soil map. The resolution of this map is 5′ over South America and uses 16 texture categories following Zobler (1986) and including some special soil types. This map was regridded to 0.25° and correlated with INPE soil map to unify categories and complete the latter for the whole South America. The final map incorporated into the Eta model is shown in Fig. 2.

Also, this soil map and the hydraulic parameters were applied in the hydrological balance model to obtain initial soil moisture conditions for Eta model integrations, as described below.

4 Eta model and sensitivity experiments

4.1 Eta model

The Eta model (Mesinger et al. 1988; Black 1994) is a limited area model which utilizes the eta vertical coordinate (Mesinger 1984). The prognostic variables are temperature, horizontal wind components, specific humidity, surface pressure, turbulent kinetic energy, and cloud hydrometeors. The convective scheme used is the Betts-Miller-Janjic scheme (Betts and Miller 1986; Janjic 1994) while the radiation package was developed by the Geophysical Fluid Dynamics Laboratory in Princeton. Shortwave radiation in the model is treated using the Lacis and Hansen (1974) scheme, whereas longwave radiation is estimated by the Fels and Schwarzkopf (1975) scheme. Initial conditions used to force the Eta model experiments are taken from the NCEP global model forecasts, whereas the lateral boundary conditions are taken from the INPE global model forecasts (Bonatti 1996) which are updated every 6 h. The Eta model is used operationally at INPE since 1996 to produce weather forecasts over South America where it has been subject to evaluations (Bustamante et al. 1999; Seluchi and Chou 2001).

The land-surface physics are resolved by a land surface model (LSM) known as Noah (Ek et al. 2003). The Noah LSM is a model of intermediate complexity for use in operational weather and seasonal prediction models, which can also be executed in an uncoupled mode. Noah simulates soil moisture (both liquid and frozen), soil temperature, snow depth, snow water equivalent, canopy water content, and the land surface energy and water fluxes. Originally, the soil model uses four layers and nine different types of soil based on the 1° × 1° database created by Zobler (1986) with soil parameters taken from Cosby et al. (1984).

4.2 Sensitivity experiments

The model was configured to run on a 40-km grid resolution with 38 unevenly distributed vertical levels, with almost half of them below 700 hPa. The model top is set to 25 hPa. Figure 1 shows the domain which includes all of South America north of 40°S and portions of the adjacent oceans. Although incompatibilities between the Eta model physics and the boundary conditions provided by the INPE global model could be expected, they have not affected our integrations because of the large domain used in our experiments. To reduce model spinup effects, initialization time was taken 48 h before the major heavy

Table 2 New values of the soil parameters in the Eta model

Soil Type	Θ_s (%)[a]	Ψ_s (m)	K_s (m/dia)[a]	B	QTZ (%)	Θ_c (%)[a]	Θ_w (%)[a]	Θ_D (%)[a]	D m^2/dia	F
1	0.16	0.27	4.28E−07	2.03	0.60	0.03	0.08	0.08	1.48E−06	−0.21
2	0.19	0.10	8.22E−07	2.78	0.25	0.04	0.16	0.16	1.21E−06	−1.00
3	0.19	0.25	1.69E−06	3.03	0.25	0.07	0.32	0.32	6.68E−06	−0.77
4	0.29	0.11	1.40E−05	2.25	0.60	0.05	0.11	0.11	1.16E−05	−0.17
5	0.29	0.09	9.45E−06	2.62	0.45	0.06	0.19	0.19	7.60E−06	−0.47
6	0.30	0.05	9.18E−06	3.02	0.25	0.06	0.27	0.27	4.90E−06	−0.88
7	0.37	0.09	7.70E−05	1.97	0.82	0.04	0.07	0.07	3.85E−05	0.13
8	0.38	0.04	3.43E−05	2.53	0.25	0.05	0.18	0.18	9.35E−06	−0.45
9	0.36	0.02	5.02E−05	2.98	0.25	0.05	0.27	0.27	7.32E−06	−1.05
10	0.32	0.43	1.71E−05	2.13	0.60	0.09	0.12	0.12	4.85E−05	0.58
11	0.32	0.4	5.28E−06	2.44	0.35	0.10	0.20	0.20	1.61E−05	0.40
12	0.30	0.22	3.46E−06	2.90	0.25	0.10	0.26	0.26	7.22E−06	−0.17
13	0.37	0.6	2.05E−05	2.01	0.60	0.12	0.11	0.11	6.77E−05	0.91
14	0.37	0.5	6.96E−06	2.42	0.10	0.13	0.20	0.20	2.30E−05	0.65
15	0.40	0.13	4.95E−05	2.97	0.10	0.11	0.28	0.28	4.95E−05	−0.05
16	0.31	0.93	3.64E−06	2.81	0.10	0.16	0.20	0.20	3.06E−05	0.54
17	0.42	1.29	1.06E−05	1.84	0.25	0.18	0.12	0.12	6.05E−05	1.41
18	0.39	0.84	6.55E−06	2.30	0.10	0.16	0.19	0.19	3.28E−05	0.98

[a] Parameters used in both the Eta model and in the soil hydrological balance model; values from the latter are taken and transformed to match units in Eta land-surface model

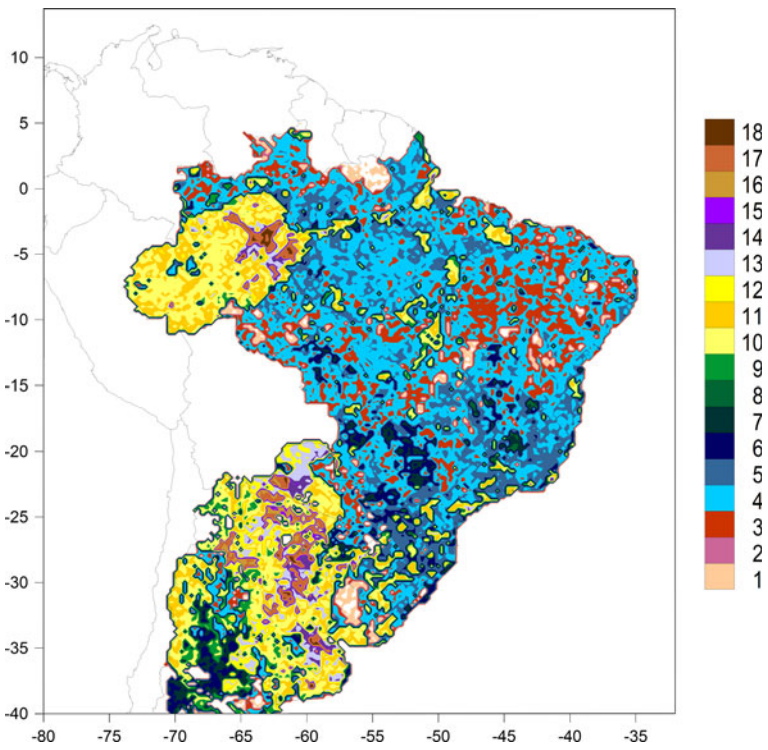

Fig. 1 Area covered by the INPE soil data base

rainfall event. Integrations continued for 48 h to capture the total lifetime of the mesoscale convective systems, MCS. Under these conditions a first control run (CTRL) is performed.

One experiment which incorporated both the new soil moisture initial conditions and the new soil map in the model run was designated as M&M. In this experiment the soil classification and parameters incorporated into Eta

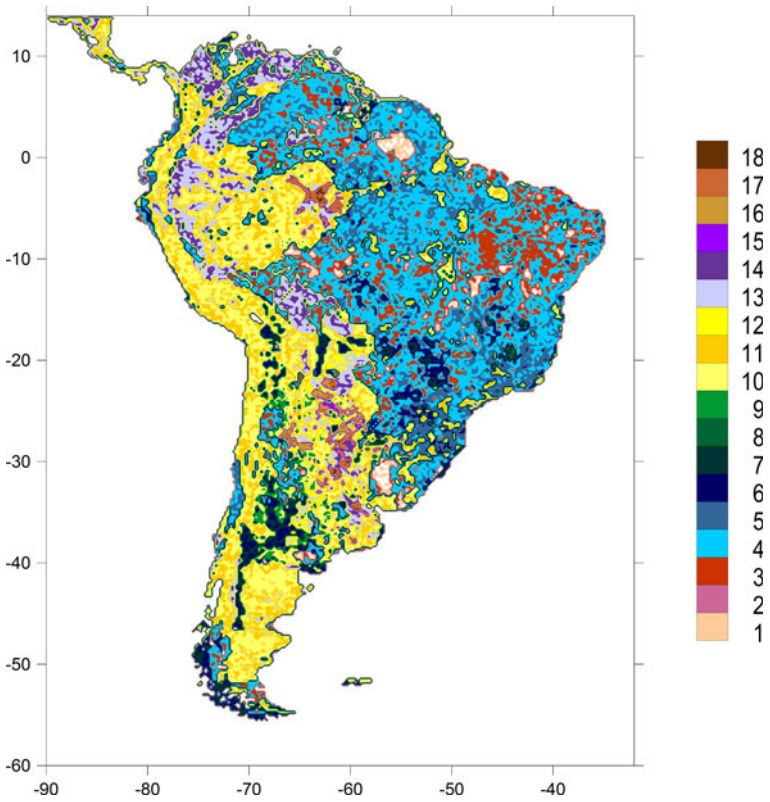

Fig. 2 New soil map included in the Eta model

model coincided with those in the INPE soil hydrological balance model which was in equilibrium. Results were compared with the CTRL run evaluating sensitivity of soil moisture on precipitation.

4.3 Quantitative precipitation verification

In order to verify the rain forecasts of each experiment against the observed precipitation produced by the mesoscale convective system the Ebert-McBride technique (EMT) is applied (Ebert and McBride 2000). It employs the concept of matching individual forecast and observed areas utilizing contiguous rain areas (CRAs), defined as the areas of contiguous observed and forecast rainfall enclosed within a specific isohyets. The aim of the CRA approach is to verify to what extent the forecast rain entity has the same location, shape, and magnitude as observed. A displacement is performed using an objective pattern-matching technique to optimally align the forecast with the observations. For 24-h quantitative precipitation forecast verification, the authors used a CRA critical rainfall threshold of 5 mm per day for the minimum accumulation required for a grid point to be considered part of a CRA. Grams et al. (2006) found that 0.25 inches for 6 h worked reasonably well at identifying an MCS in the central United States. Here, 30 and 50 mm per day thresholds were used to identify the convective system.

5 Synoptic situation

On October 10th 2006, a Mesoscale Convective System (MCS) developed over northern Argentina and moved towards the southern states of Brazil. This system caused heavy rainfall, strong winds, hail, and floods in both countries. On October 8th a baroclinic trough was situated to the north of Argentina and was started to move eastwards in direction to the state of Rio Grande do Sul in Brazil. A cold front is positioned over the southernmost part of the province of Buenos Aires at 0000 UTC on October 10th moving northeastward and reaching the northern part of the province 12 h later (Fig. 3a). At this point the frontal cloud band extended northwards covering the province of Santa Fe, in eastern Argentina. At 1800 UTC October 10th, a low pressure center developed in northern Argentina and caused strong uplifting in the region and in southern Brazil (Fig. 3b). The high values of dew point temperatures over central Paraguay, central-east Argentina, and northern Uruguay exceeded 21 °C, and indicated the presence of very moist and warm air provided by northerly winds from the Amazon region. The strong gradient of the dew point temperature over the province of Buenos Aires, Argentina, was related to the presence of the cold front, while in southern Brazil the weaker dew point temperature gradient was associated with the formation of a surface

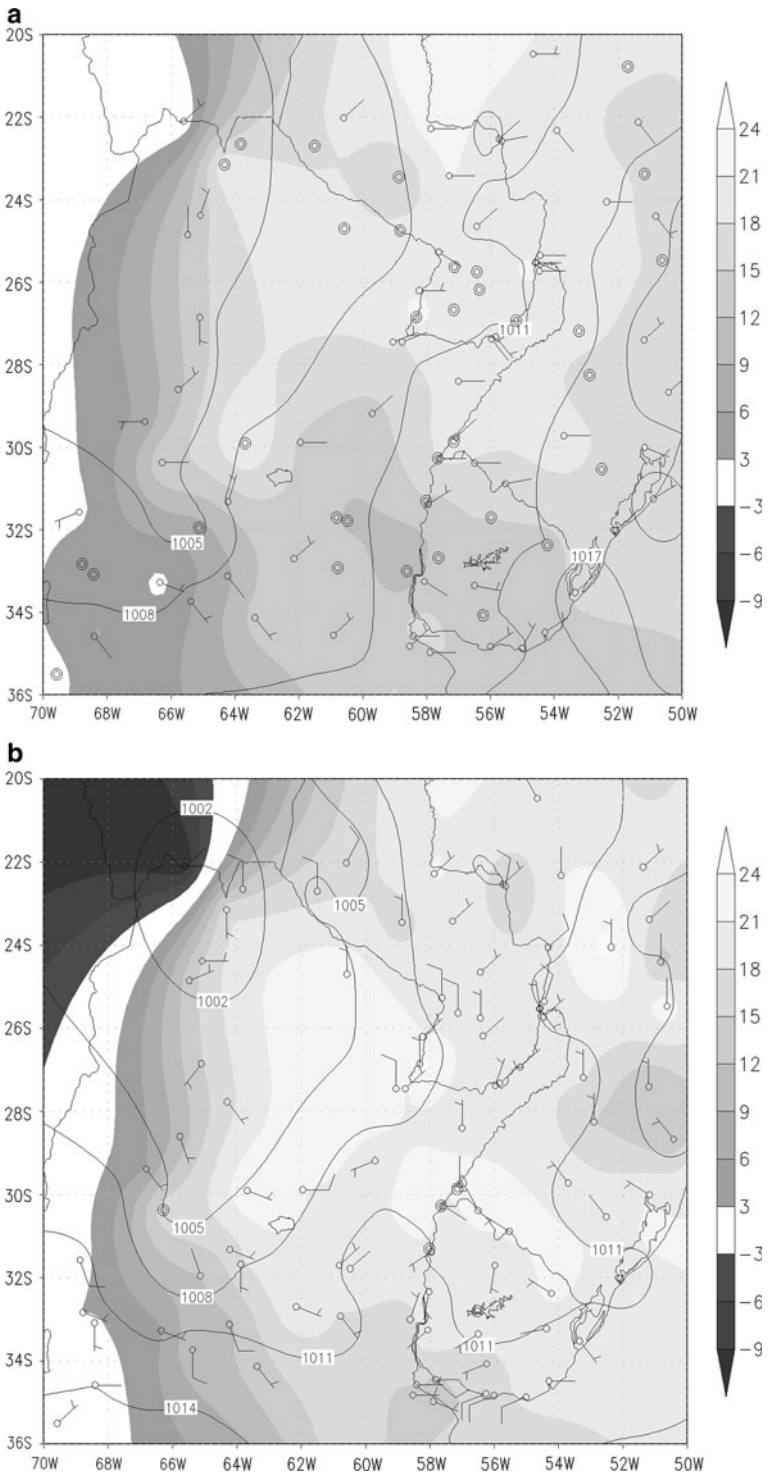

Fig. 3 Mean Sea level pressure, surface dew-point temperature (K) and wind (m/s) for the synoptic situation at **a** 0000 UTC, and **b** 1800 UTC on October 10th 2006, **c** 200 hPa geopotential height (m) and wind (m/s) at 1200 UTC on October 11th

frontal wave. At upper levels, the subtropical jet crossed north-central Argentina in the NE–SW direction (Fig. 3c) and divergence values were observed at the left of its exit region, over most of the border between Uruguay and Brazil extending over Argentina, in agreement with the area with the most intense precipitation.

6 Results

During the first 48 h of the runs no precipitation was forecasted over Argentina, Uruguay, southern Brazil, and Paraguay, particularly over the area where the MCS was to develop. This case allows a clear insight into the role of

Fig. 3 continued

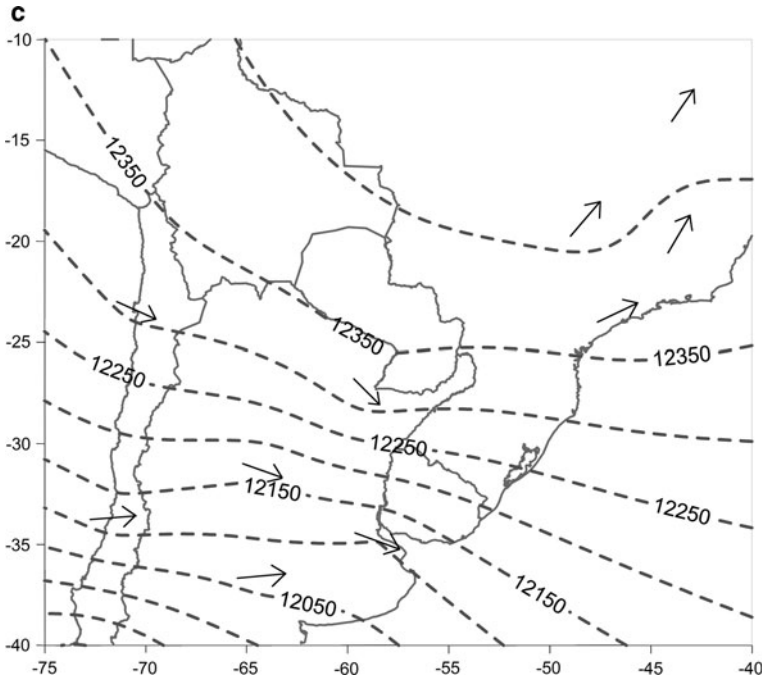

changes to the surface soil conditions on different atmospheric variables.

6.1 Initial soil moisture availability

The initial soil moisture availability (i.e. the available water between wilting point and saturation conditions) in each experiment run is shown in Fig. 4. Areas over eastern Argentina and Paraguay, Uruguay, and most of southern Brazil are at saturation conditions in the CTRL run, clearly distinguished from the dry conditions in the western areas by an intense gradient, where there was practically no soil moisture available.

The strong gradient is not evident in M&M run. Soil moisture was mostly below 50 % in the M&M experiment with dry conditions over most of Argentina, Bolivia, Paraguay, and Chile and higher moisture availability over Uruguay, Brazil, southern Paraguay, and NE Argentina. However, the field did not exhibit soil moisture availability values below 20 %; therefore, the new soil moisture initial conditions and the use of a new soil type distribution created wetter conditions in dry areas and moisture availability below saturation in the humid region.

The temporal variations in these initial soil moisture availability, SMAV, fields during each of the experiments were small and in general are not affected by the convective event, since the variations in soil moisture availability were approximately 10 % in the area of most of the rainfall (not shown).

6.2 2-m temperature

The initial soil moisture availability fields have a direct influence on the determination of the temperature field at 2 m in each experiment. The differences between the experiments created different temperature forecasts. Figure 5 presents Hovmoller diagrams at 30°S for the forecasted temperature at 2 m in CTRL experiment and the difference between M&M experiment and CTRL. There was a faster nocturnal cooling in M&M experiments with respect to CTRL in the area east of 63°W, with highest values where moisture availability was approximately 90 % in CTRL, below 30 % in M&M. These drier conditions induced a faster warming over this area in the morning hours of these experiments, with temperature differences of up to 4 °C in M&M with respect to CTRL.

On the other hand, west of the strong SMAV gradient area in CTRL experiment, the differences in diurnal cycle of temperature show opposite signs to soil moisture. During day time, the wetter M&M soil moisture conditions damp the temperature raise resulting in negative differences but lead to warmer nights.

Two stations in Argentina were selected to validate temperature forecasts where observations are available every 3 h: Ceres (29.88°S, 61.95°W) and Paso de los Libres (29.86°S, 57.15°W). The nearest model grid box centered at 30°S, 61.8°W and 30°S 57°W, both included in Fig. 5, were used for comparison. Forecast hours for each experiment were selected to match the local time observations. Ceres, which is located closer to the strong SMAV

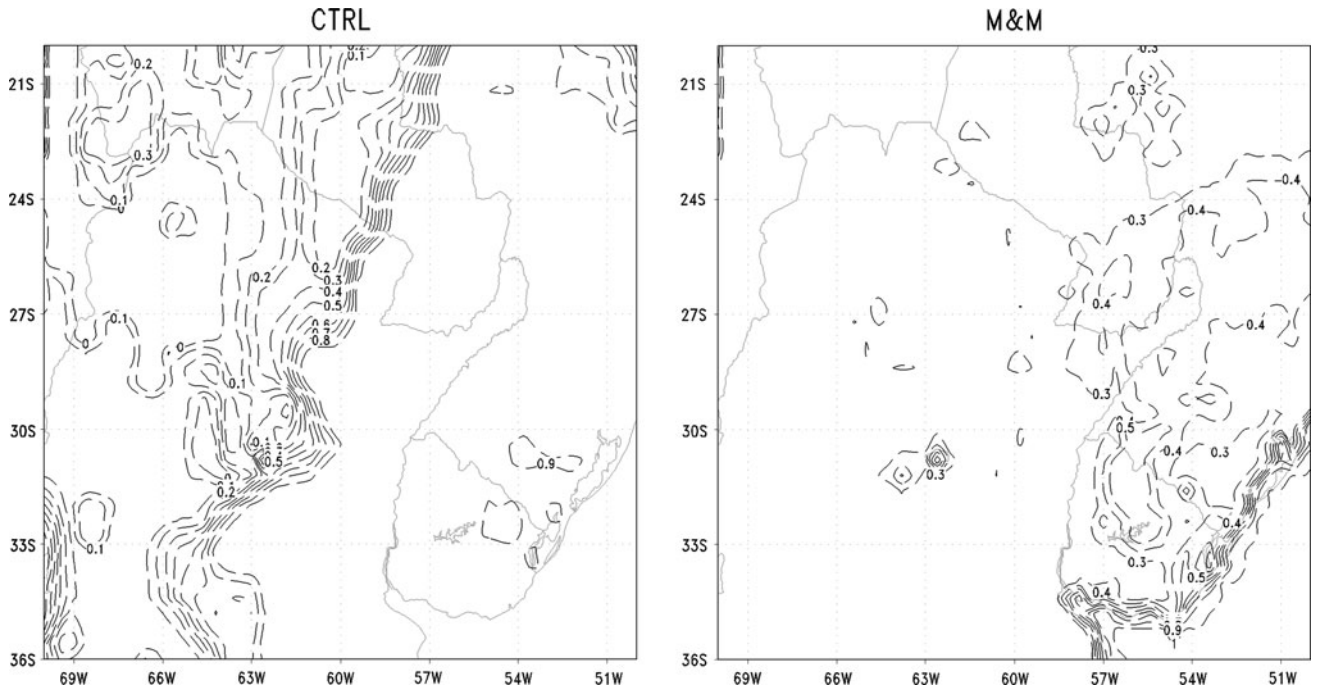

Fig. 4 Soil moisture availability (%) initial conditions 0100 UTC 8 October 2006 for CTRL (*left*), and M&M (*right*) experiments

gradient area, exhibits low SMAV values (9.8 %) after 1 h of integration in the CTRL experiment, whereas in M&M experiment, soil moisture is almost 25 %. At Paso de los Libres grid point, which is close to the border of Argentina, Uruguay, and Brazil, the SMAV initial values are much higher in CTRL (84 %) whereas there is little change in M&M (26 %).

A measure of the errors between the observed and forecasted 2-m temperature at each location is shown in Table 3. The diurnal cycle of temperature seems to be best represented by the CTRL experiment both at Ceres and Paso de los Libres stations, as seen by the errors (Table 3). The two first 2-m temperature cycles in all experiments closely follow observations (Fig. 6); during the following hours rain is forecasted by each experiment at different times and with different volumes, thus modifying in different ways the diurnal cycles of the rest of the integration, and generating the greatest differences in comparison with observations.

6.3 Vertical atmospheric structure

The approaching cold frontal system was revealed by the appearance of high clouds in all runs on October 9th. These clouds developed in an atmosphere characterized by a three-layer vertical structure: a moist layer between 300 and 200 hPa where relative humidity (RH) was above 60 %, a dry mid-troposphere where RH was lower than 20 %, and finally, a more humid boundary layer which increased its moisture content and extended vertically during the following 24 h according to the soil moisture conditions. Wet surfaces used most of the absorbed energy to evaporate water, increasing the near-surface specific humidity, whereas dry surfaces would be heated due to absence of evaporation. The Bowen ratio was low over wet surfaces, given by large latent heat flux and small sensible heat flux, while opposite magnitude of fluxes were observed over surfaces with small soil moisture availability and were characterized by a high Bowen ratio.

Figure 7 illustrates, for each experiment, the vertical distribution of relative humidity and the evolution inside the boundary layer of model grid point centered at the 34°S 64°W. The experiment (CTRL) with highest SMAV content in this region developed the most humid conditions, at around 1200 UTC where the whole column exhibited relative humidity values above 70 % between surface and 200 hPa. The M&M experiment, where SMAV values were below 25 %, had high relative humidity core at 1200 UTC on October 10th but the values in the lower atmosphere were in general below 70 %. This dry mid-tropospheric layer laying over a moist and warm boundary layer is an important factor for the future development of severe thunderstorms since air entrainment above 700 hPa can cause high evaporation and intensify downdrafts.

Convective rainfall was triggered earliest in the CTRL simulation, as rain started at 0800 UTC (5am LT) on October 10th at 34°S 64°W. At this point, both soil moisture and the column of air between surface and

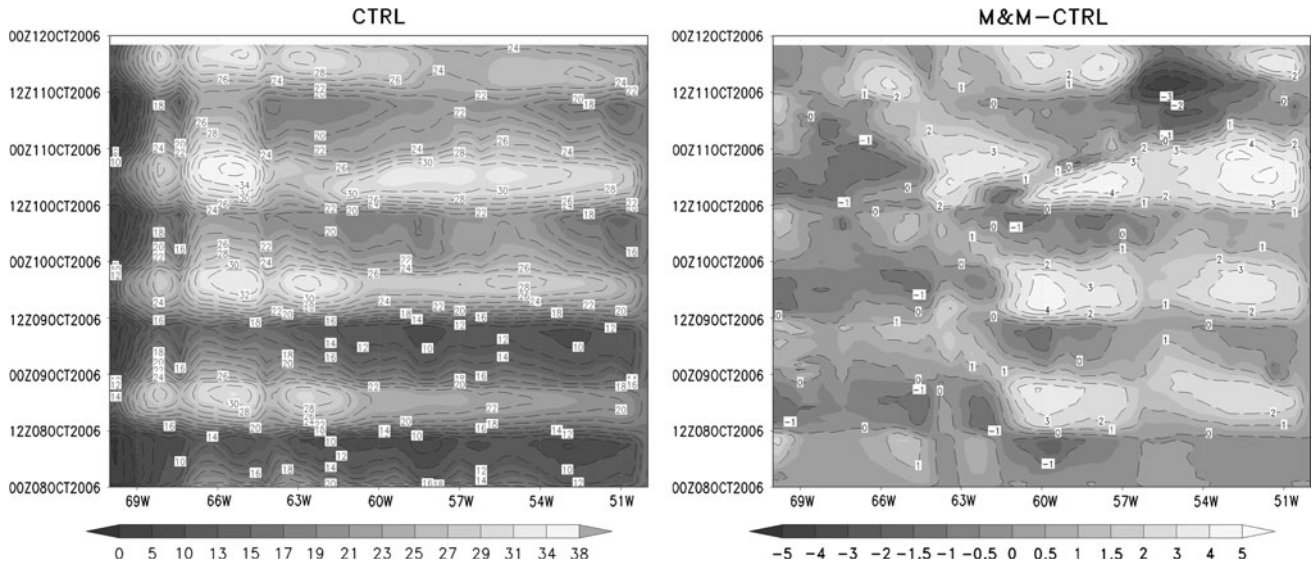

Fig. 5 Hovmoller diagram of 2-m temperature (°C) at 30°S for the CTRL (*left*) run, and differences between M&M and CTRL (*right*) experiments

Table 3 Temperature Bias (°C), RMSE (°C) and MAE (°C) of CTRL and M&M experiments verified against observations Ceres and Paso de los Libres stations

	Ceres		Paso de los Libres	
	CTRL	M&M	CTRL	M&M
BIAS	1.20	1.73	0.32	1.36
00 UTC	1.24	2.63	1.94	4.19
06 UTC	1.76	2.73	0.24	0.44
12 UTC	1.31	1.26	−0.65	−1.01
18 UTC	0.65	0.50	−0.91	1.57
RMSE	2.14	3.02	2.86	3.44
MAE	1.72	2.35	1.99	2.26

200 hPa had relative humidity values above 70 % (Fig. 7). The weaker downward sensible heat flux during night hours caused the temperature difference between 925 and 1,000 hPa to be always negative in the CTRL.

During the night hours M&M developed a strong temperature inversion due to the strong sensible heat flux from the atmosphere to the ground. Betts et al. (1994), Betts and Ball (1995) demonstrated using observational data and a simple boundary layer model that reduced evaporation, and, therefore, increased heating at the surface, increases entrainment at the top of the boundary layer and thus increases entrainment of low-θ_e air from above the boundary layer. This leads to lower θ_e in the boundary layer and a more stable troposphere, which may, therefore, lead to less convective precipitation. The equivalent potential temperatures in the M&M experiment (Fig. 8) exhibited the described behavior in response to the low evaporation and high heating arising from low SMAV values. Consequently, no convective rainfall was forecasted by this experiment in this area at this time.

Based on two measures of atmospheric thermodynamic properties, the convective triggering potential (CTP), a measure of the temperature lapse rate between 100 and 300 hPa above the ground surface, and a low-level humidity index (HI_{low}), Findell and Eltahir (2003b) presented a framework for describing atmospheric controls on soil-moisture boundary-layer interactions. It allowed to distinguish between three different types of early-morning atmospheric conditions: those favoring moist convection over dry soils (CTP $\geq$200 J/kg and $HI_{low} \geq 11°$ C), those favoring moist convection over wet soils ($0 \leq$ CTP $\leq$200 J/kg and $5 \leq HI_{low} \leq 12°$ C), and those that would allow or prevent deep convection activity during the day, independent of the surface energy flux partitioning. The early morning (0900 UTC) thermodynamic conditions described by these properties were obtained for both experiments on October 10th (Fig. 9). Over wet soils, east of the SMAV gradient (CTRL, Fig. 4), convection during the evening hours should be expected with positive CTP below 200 J/kg and a low-level humidity index between 5 and 12 °C. Conditions favoring moist convection over the dry soils, both in CTRL and M&M, were not fully accomplished. Although there were areas with HI_{low} values within the expected range, the convective triggering potential was well below 200 J/kg.

In a companion paper (Findell and Eltahir 2003a) the authors included in their framework the effect of winds in the boundary layer on enhancing or prohibiting the likelihood of convection. Winds veering, i.e. wind rotating with

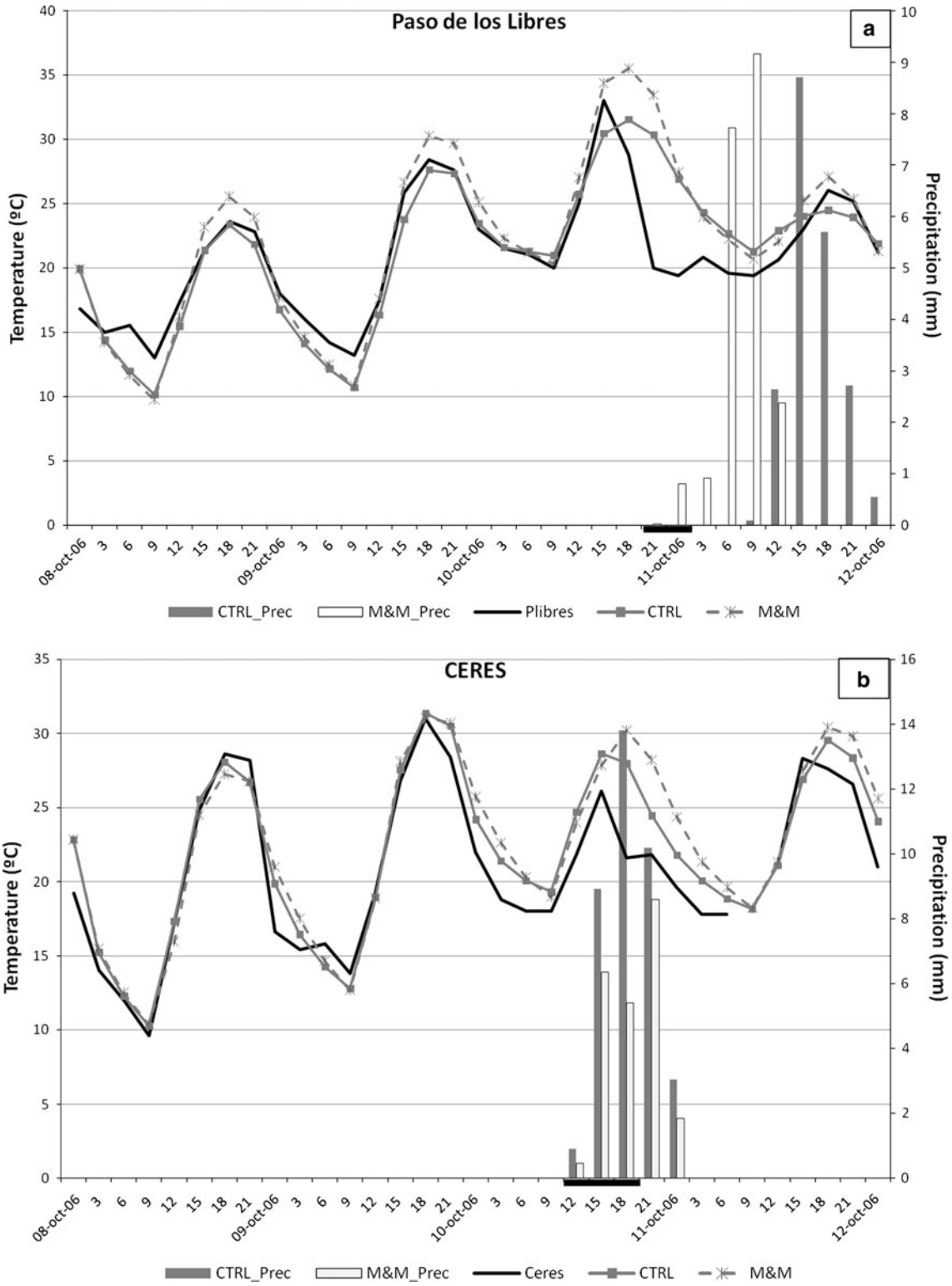

Fig. 6 Forecasted and observed 2-m temperature (*lines*, °C) and forecasted precipitation (*bars*, mm/3 h) every 3 h at **a** Paso de los Libres (29.86°S, 57.15°W), and **b** Ceres (29.88°S, 61.95°W). *Thick horizontal line* on date axis indicates observed rainfall period

height opposite to planetary rotation (anticlockwise in the southern hemisphere), in the lowest 300 hPa can enhance convection since they contribute with additional buoyancy to the boundary-layer air. This new feature could have contributed to the development of convection in both experiments since wind veering occurred in the area where

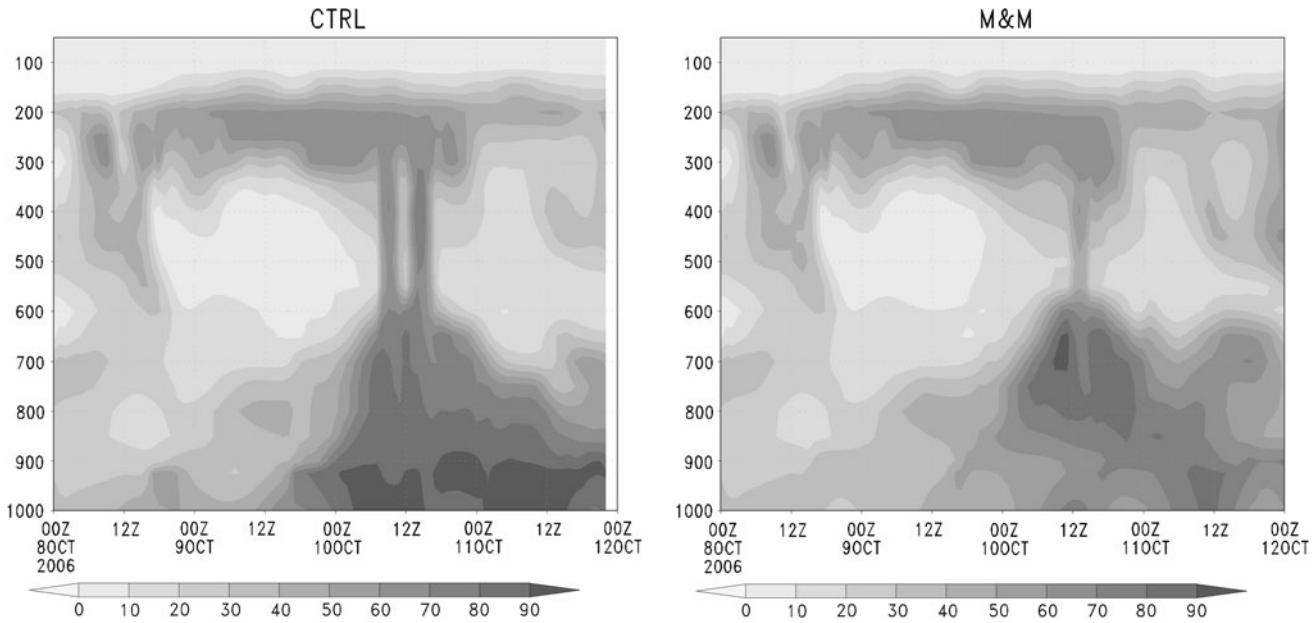

Fig. 7 Vertical and temporal evolution of relative humidity of model grid point at 34°S 64°W. CTRL (*left*), and M&M (*right*) experiments

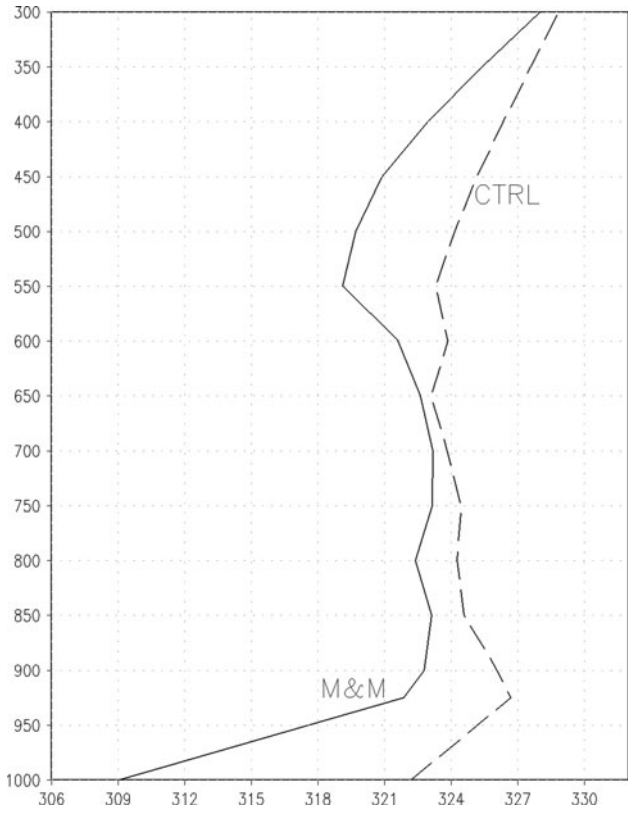

Fig. 8 Equivalent potential temperature (K) profile at 0800 UTC October 10th for model grid point centered at 34°S 64°W

convection developed. However, this framework is mainly applicable to cases when convection developed during the evening hours. In this case, although the first signs of convection appeared at different times and places in each experiment, in all cases convection started before midday; therefore, this framework does not completely explain the the origin of convection.

At 1200 UTC, signs of convection appeared in M&M at 31.7°S 61°W, northeast of the first signs of convection in CTRL and southeast of the new cells. By 1800 UTC all experiments had developed convection in areas varying from central to eastern Argentina and reaching eastern Uruguay (Fig. 10). An intense low-pressure system had developed in northwestern Argentina and a trough with NW–SE direction crossed most of Argentina and entered Uruguay in CTRL south of the border with Brazil, while in M&M the trough was located over the border. Precipitation developed downwind of this trough; hence there are differences in the location of the forecasted rainfall.

The development of convective clouds and precipitation is related to the convective available potential energy (CAPE), which is the amount of energy available to an air parcel to ascend once it has reached the level of free convection. When CAPE is large, the atmosphere will be more unstable. Schär et al. (1999) concluded that wet soils increase the efficiency of convective precipitation processes, including an increase in convective instability. However, convection depends also on the convective inhibition (CIN), that is, the amount of energy needed to supply an air parcel to elevate it up to the level of free convection. Large values of CIN imply large resistance to convective development. Therefore, the more favorable conditions for convection and precipitation are identified by large values of CAPE and small values of CIN, as can be seen in Fig. 11. Both experiments developed convection

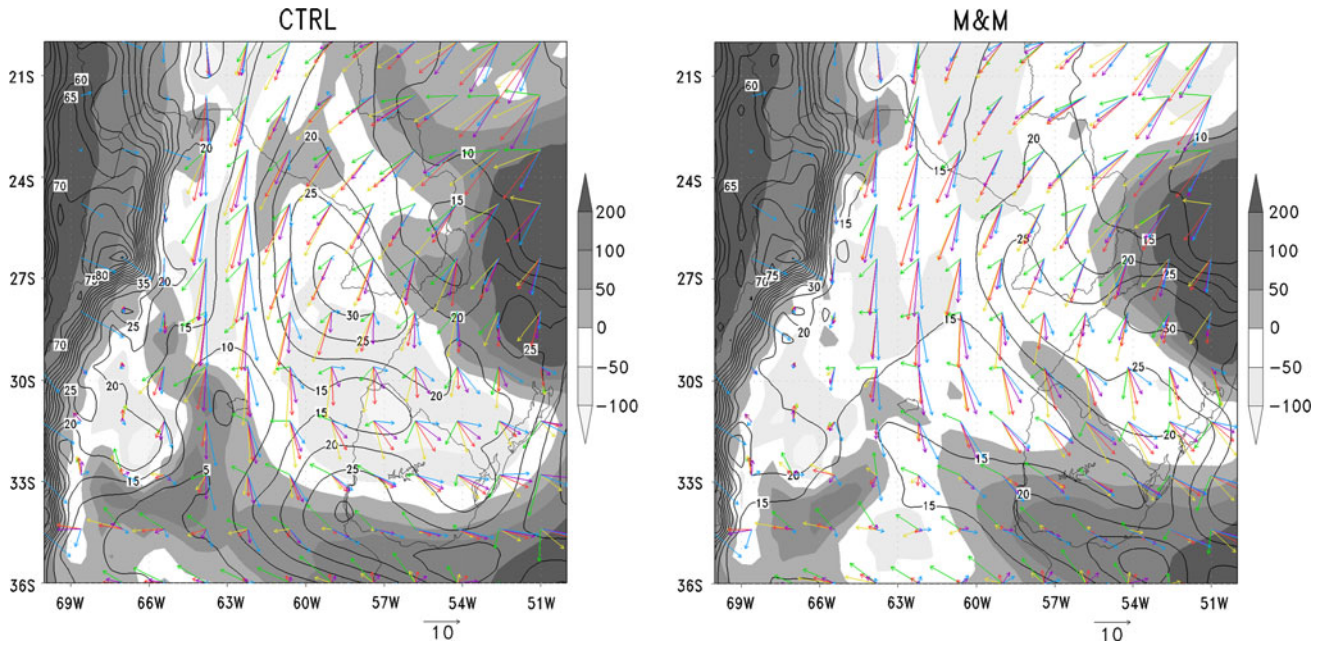

Fig. 9 Convective triggering potential (J kg^{-1}) (*shaded*), low-level humidity index (°C) (*lines*) and winds (ms^{-1}) between surface and 700 hPa at 0900 UTC 10 October 2006 for CTRL (*left*) and M&M (*right*) experiments. Wind levels: 1,000 hPa (*green*), 900 hPa (*yellow*), 850 hPa (*red*), 800 hPa (*violet*), and 750 hPa (*blue*)

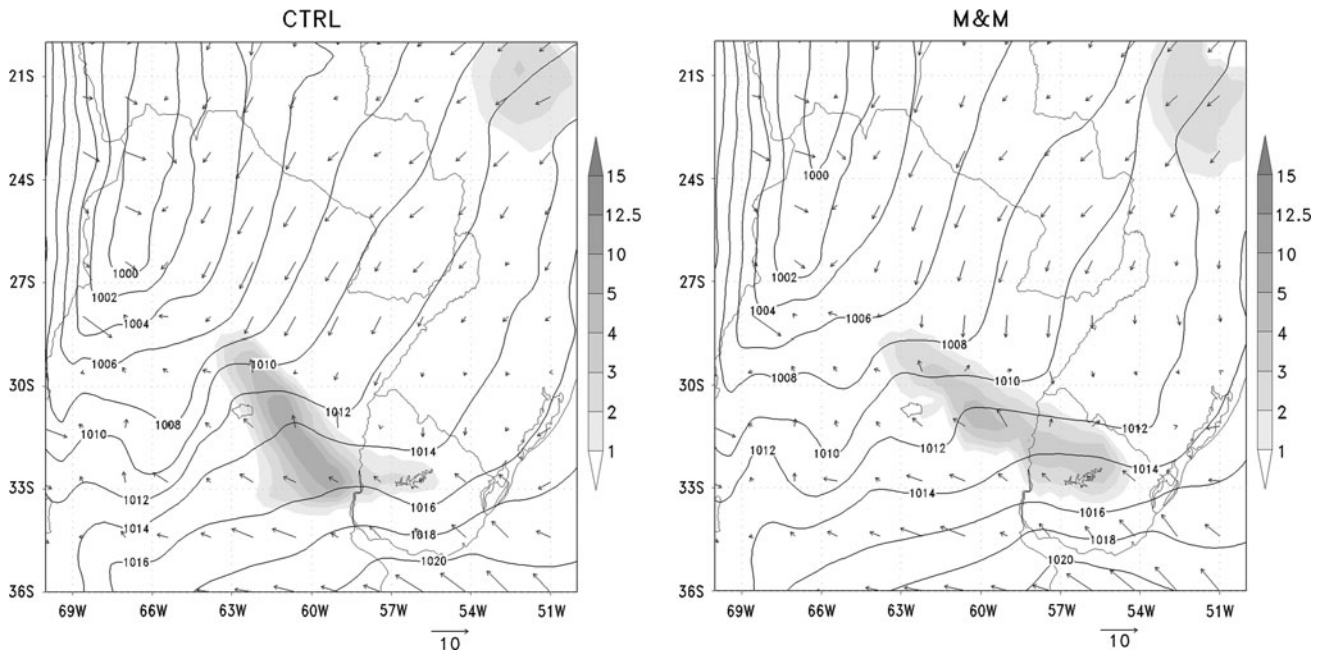

Fig. 10 Mean Sea level pressure (hPa), 10-m wind (m/s), and precipitation (mm/day) conditions at 1800 UTC 10 October 2006 for CTRL (*left*) and M&M (*right*) runs

not in the area where highest CAPE values were forecasted but where the lowest CIN values were found.

Aloft, the core of a jet stream was observed at 250 hPa over Buenos Aires province extending over the Atlantic Ocean. Riehl et al. (1952) asserted that divergence fields associated with wind speed maxima (i.e. jet streaks) in the upper-level jets produce upward motion in the left front (right front in the southern hemisphere) and right-rear (left-rear in SH) quadrants of the streak. This is consistent with the divergence pattern observed in Fig. 12, with strong upward movements at 500 hPa (not shown) and the rainfall area. Beebe and Bates (1955) emphasized role of the

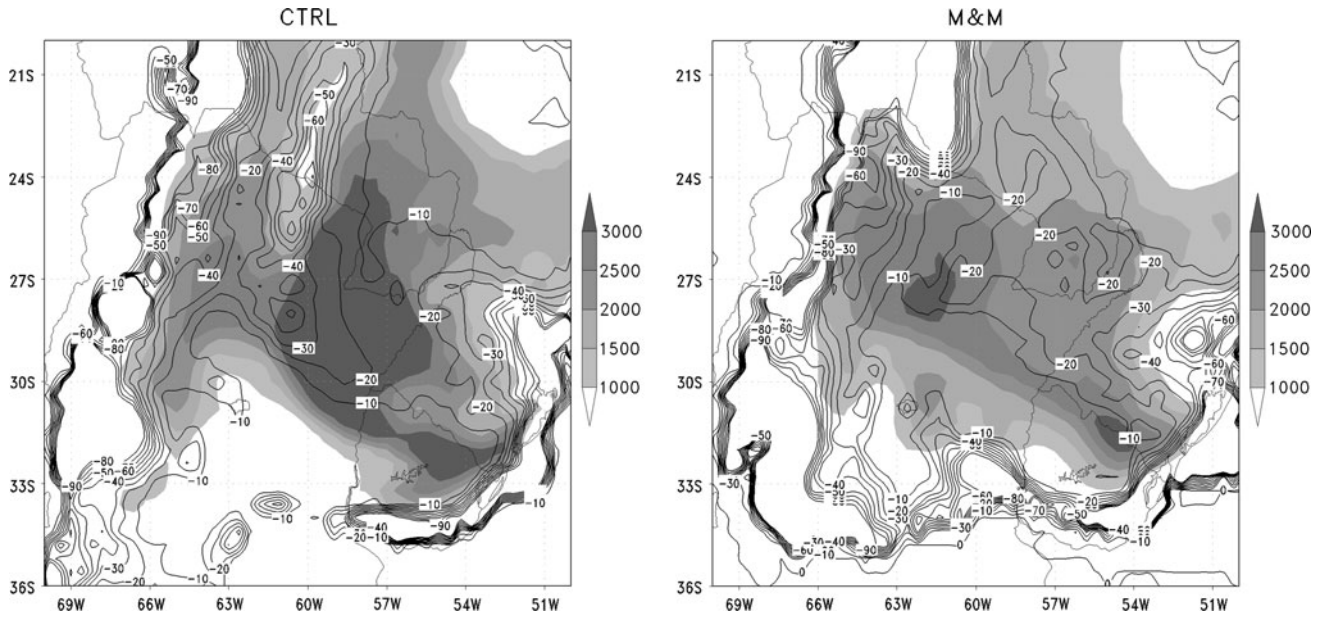

Fig. 11 Convective available potential energy (CAPE, *shaded*) and convective inhibition (CIN, *contours*) at 1800 UTC 10 October 2006 for CTRL (*left*) and M&M (*right*) experiments. Units are J/kg

interaction of streaks in upper-level jet and the low-level jet (LLJ) in the development of severe thunderstorms. The dashed lines in Fig. 12 show that the convective storms were occurring at the nose of the LLJ maximum (dashed lines), a couple of hundred kilometers north of the upper jet streak (solid lines). The intense northerly low-level flow had been blowing steadily during the previous 24 h incorporating moisture and heat from low latitudes, which are necessary for the MCS development. The soil conditions impacted not only on the intensity of this LLJ but also on its direction and extent. The strongest winds were found in CTRL experiment, with values above 12 m/s, while the 9 m/s isotach extended further south when compared with the other experiment. The wind shear associated with the rainfall area was rather weak, with lowest values in CTRL experiment.

6.4 Precipitation

During the following hours the storms continued to develop and the precipitation area advanced over Uruguay. In the CTRL experiment, precipitation area seemed to be more stationary extending northeasterly and southwesterly but never reaching the border between Uruguay and Brazil, where storms were observed producing hail, intense downdrafts, and even some floods. At 2100 UTC a new storm area developed to the northeast of the storm line. The rainfall core was located in the same area in both experiments; however, CTRL presented higher values and the storm was restricted to a relatively smaller area than in M&M. The storm moved with a northeast component during the following hours; however, in CTRL the storm displaced with a NNE component while the prevailing component was ENE in the other experiment.

Figure 13 depicts the accumulated rainfall for each experiment between 1200 UTC October 10th and 1200 UTC October 11th. It is clear that CTRL, the experiment with highest soil moisture conditions in the eastern half of the domain, developed the highest amount of rainfall. However, the orientation of the rainfall area differed considerably from M&M laying backwards with respect to the storms observed over eastern Argentina, northern Uruguay, and southern Brazil (Fig. 14). The storm developed in northwestern Argentina had precipitation overestimated by CTRL and also misplaced westward from the 92 mm maximum registered by Presidencia Roque Saenz Peña. In this sense, M&M is the experiment with the best forecast, both in proximity and intensity of this rainfall area.

To estimate the displacement error and to verify the location-corrected rain forecast produced by each experiment as well as their shape and magnitude, the EMT was applied. The verification statistics presented in Table 4 summarize the overall skill of each experiment in forecasting the observed rainfall on October 10th. M&M has the smallest MAE, and RMSE, the highest probability of detection, spatial correlation coefficient, and bias score as well as the lowest false-alarm probability. This last statistics measures the ratio of the predicted rain area to the observed, without regard to forecast accuracy. The bias score of this experiment is closest to 1 indicating that the area with forecasted rain is closest to the observed.

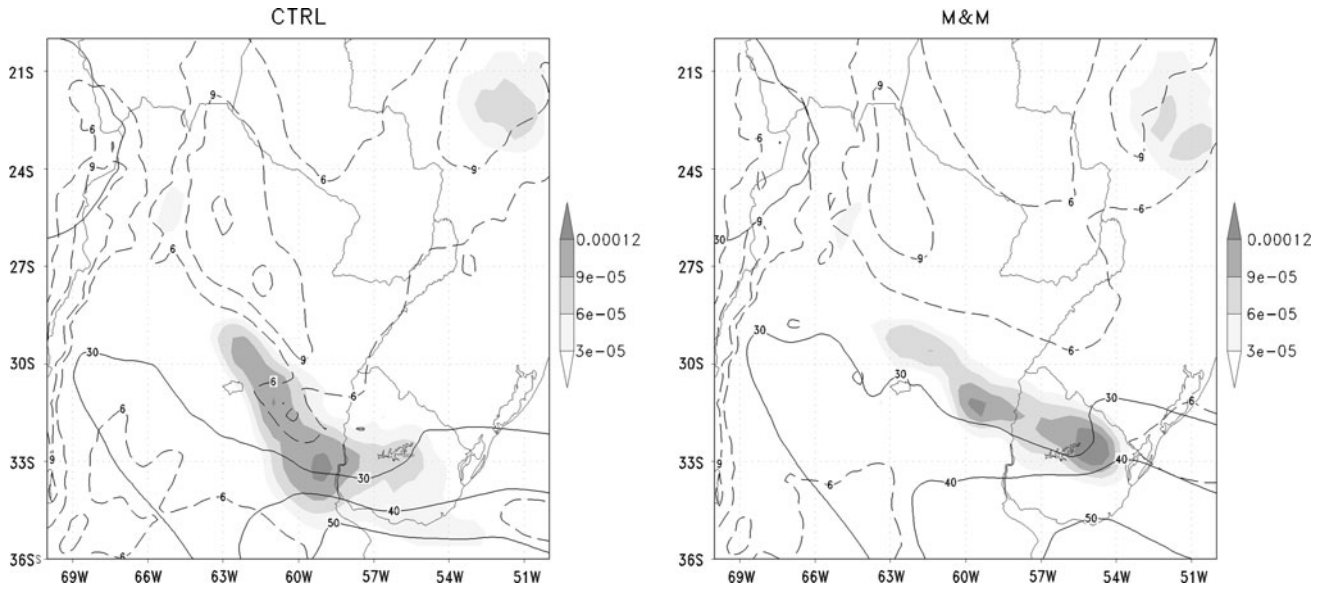

Fig. 12 250-hPa wind divergence (*shaded*; 1/s), 250 hPa wind intensity (*solid lines*; m/s), and 850 hPa wind intensity (*dashed lines*; m/s) at 1800 UTC 10 October 2006 for CTRL (*left*) and M&M (*right*) experiments

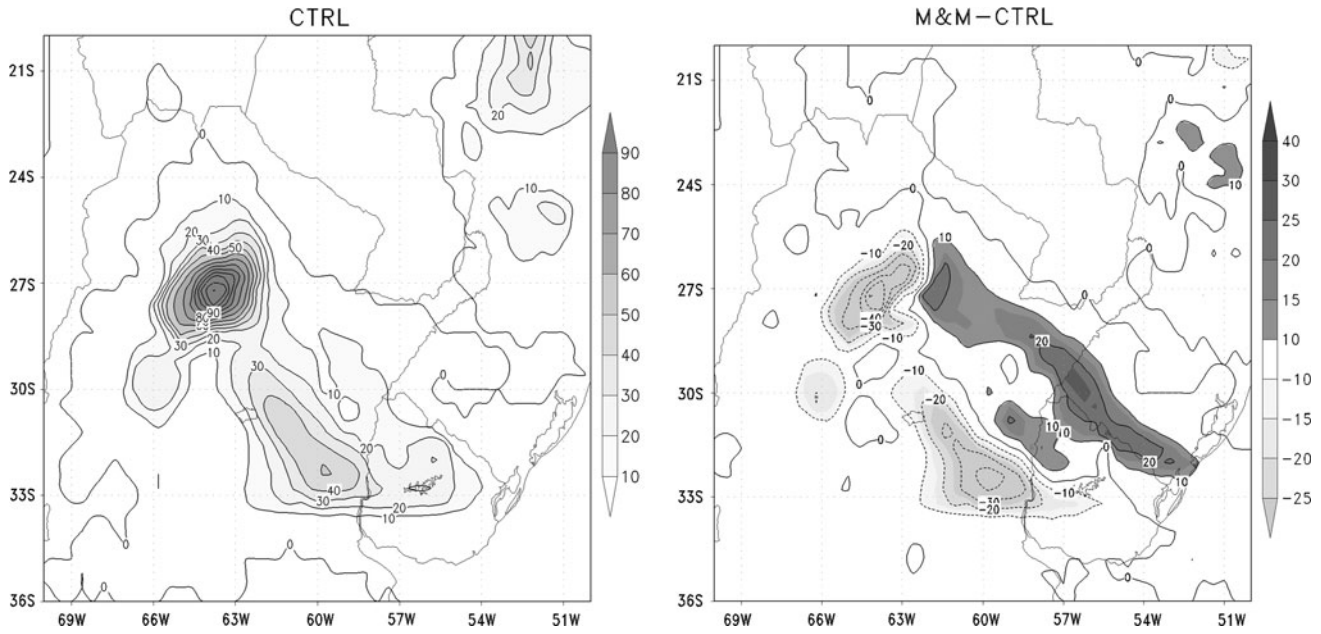

Fig. 13 Accumulated precipitation (mm/day) between 1200 UTC 10 October and 1200 UTC 11 October for CTRL (*left*), and difference between M&M and CTRL (*right*) experiments (mm/day)

In EMT the horizontal displacement of the forecast is determined by translating the forecast rain field until the total squared difference between the observed and forecast fields is minimized. This allows a decomposition of total error into components due to (a) location; (b) rain volume, and (c) pattern. Following Grams et al. (2006) a 30-mm/day threshold is considered to work considerably well in identifying the MCS in all experiments. However, this implies that areas compared differ in each case since the forecasts of each experiment present different patterns as shown in Fig. 13. Results are summarized in Table 5. The precipitating system was placed by both experiments west of the observed pattern and slightly to the south, but the shift was smaller in M&M. With regard to the maximum precipitation, they both presented values above the 87.6-mm maximum precipitation of the observed field; however, M&M overestimated by only 3.3 % while for CTRL the difference was almost 47 %. Traditional verification

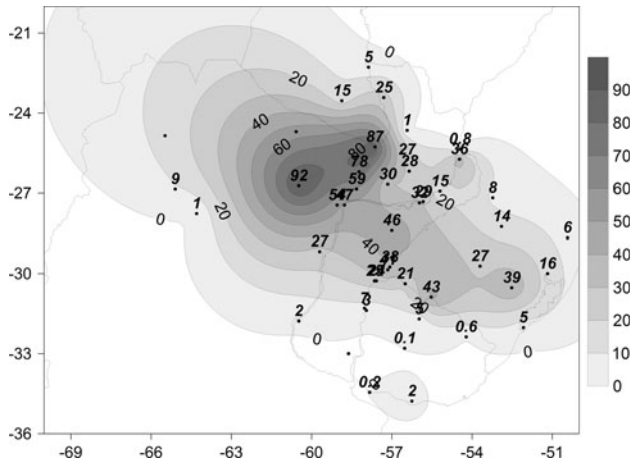

Fig. 14 Observed accumulated precipitation at 1200 UTC October 11th 2006. Maximum rainfall at Presidencia Roque Saenz Peña (92 mm/day)

Table 4 Verification statistics of total rain forecasted fields and observed on 10th October 2006

Experiment	MAE	RMS	R	Bias score	Probability of detection	False alarms
CTRL	12.8	21.35	0.086	0.776	0.362	0.534
M&M	10.27	17.54	0.309	0.854	0.499	0.416

The area considered is the one shown in Fig. 14

statistics severely penalize a mislocated QPF, with low or negative correlation coefficients and high RMS errors as can be seen in Table 5. The decomposition of QPF errors indicate that displacement and pattern errors have a lower contribution to total error in M&M than in CTRL, while the contribution of volume error is greatest in M&M. Nevertheless, total RMS error is lower in M&M.

If a more restrictive threshold is considered, 50 mm per day, M&M still has the smallest RMS error as well as the smallest pattern and displacement errors. The latter is slightly higher than in the previous case, consequently, resulting in a smaller pattern as well as in a decrease of the volume error which nevertheless is still greater than in CTRL.

Paso de los Libres and Ceres stations were also used to verify the 3-hourly evolution of rain. However, since only total values were available once the event had ended it was only possible to compare the starting hours, duration, and total volume of each experiment in the nearest grid point at each station. Bars in Fig. 6 indicate the total 3-hourly precipitation produced by each experiment. The thick short line on the hour axis indicates the duration of the observed precipitation at each station, At Paso de los Libres storms that were first reported at 2100 UTC October 10th and 41 mm were reported to have fallen 3 h later. Only M&M correctly forecasts the hour of the first storms; however, the

Table 5 CRA statistics considering 30 mm/day and 50 mm/day thresholds, the latter in brackets

	CTRL	M&M
Maximum Rain (mm)	128.47	90.50
Displacement [E, N]	[−4°,−1.20°] ([−3.6°,−0.8°])	[−2.8°,−1.20°] ([−2.8°,−0.8°])
Correlation Coef.	−0.525 (−0.803)	−0.324 (−0.669)
RMS error (mm/day)	45.72 (63.12)	40.28 (55.6)
Displacement error	69.9 % (76.3 %)	50.0 % (59.9 %)
Volume error	12.0 % (11.4 %)	38.4 % (34 %)
Pattern error	18.1 % (12.2 %)	11.6 % (6.1 %)

duration, 16 h, is much longer and the total amount of precipitation forecasted, 21 mm, is almost half the observed. The CTRL experiment forecasted rains starting 12 h after the first storms were observed with excessive duration and underestimated total rain.

At Ceres station the first storms were first reported at 1200 UTC on October 10th and ended by 1800 UTC registering 11 mm during this period. The starting hour was correctly predicted by M&M and CTRL experiments; however, they both overestimated the duration by 6 h while the total precipitation was doubled by M&M (23 mm) and tripled by CTRL (37 mm).

7 Conclusions

The results presented here have described the evolution of a Mesoscale Convective System which developed in October 2006 over northern Argentina. The convective system was simulated by the Eta model using different initial soil moisture conditions and soil maps. The new soil moisture conditions, which were used to initialize the M&M run, were taken from the operational hydrological balance model running at INPE, and represented a more accurate situation since more detailed soil and precipitation data in the area were included in the hydrological balance model. This soil information, which was used to classify soil types in the region into 18 categories of the new soil map, was included in M&M run. The soil and hydrological parameters used by the hydrological balance model were transformed to match the units of these parameters in the NOAH land-surface scheme used by the Eta model. The moisture availability field of the CTRL run was characterized by a strong north–south gradient which divided the eastern humid region from the western dry landscape. The inclusion of the new map and the new initial soil moisture conditions suppressed this strong gradient feature by creating a more homogeneous soil moisture availability field. Hence, when these modifications are included in the Eta

model, drier areas present higher moisture availability while near-saturation areas are considerably reduced.

The impact of these soil moisture availability conditions on different variables was analyzed. Temperature at 2 m cooled faster at night in the experiments including the new soil moisture conditions (M&M) over the areas where CTRL soil moisture conditions were approximately at saturation levels. Moreover, the diurnal warming was also more pronounced in M&M run where temperature differences of 4 °C were found.

The areas where higher temperatures were forecasted also presented higher sensible heat fluxes, lower latent heat flux, and lower specific humidity, and thus a higher Bowen ratio. The distribution of the Bowen ratio created a dynamic response in the mass field and, consequently, in the orientation and location of the forecasted precipitation areas.

The CTRL experiment, with highest atmospheric and soil moisture, forecasted the strongest rainfall intensities, exceeding the observed values and placing the MCS farthest to the west of the observed situation. The inclusion of a new soil map and more accurate soil moisture initial conditions, as represented by the M&M run, improved the forecast both in intensity and location of the MCS, as demonstrated by the smaller pattern and displacement errors as well as smaller RMS errors in M&M. Based on the position and pattern of the rainfall and the metrics obtained by EMT M&M was considered the best run in representing the MCS development in October 2006 over Argentina.

The work presented here discusses a sensitivity case of the influence of soil type and soil moisture on the development of MCS. However, as stated by Koster et al. (2009), the soil moisture state simulated by a land-surface model is a highly model-dependent quantity, meaning that the direct transfer of one model's soil moisture into another model can lead to a fundamental, and potentially detrimental, inconsistency. Further work is necessary to best apply soil moisture products across different models.

Acknowledgments This work was supported by the Conselho Nacional de Desenvolvimento Científico e Tecnológico (CNPq, Brazil) under Grant 490387/2006-3. The authors are most grateful to Paul Dirmeyer for all his comments and suggestions which have helped improve this manuscript.

References

Aligo EA, Gallus WA Jr, Segal M (2007) Summer rainfall forecast spread in an ensemble initialized with different soil moisture analyses. Wea Forecast 22:299–314

Beebe RG, Bates FC (1955) A mechanism for assisting in the release of convective instability. Mon Wea Rev 83:1–10

Betts AK, Ball JH (1995) The FIFE surface diurnal cycle climate. J Geophys Res 100:25679–25693

Betts AK, Miller MJ (1986) A new convective adjustment scheme. Part II: single column tests using GATE wave, BOMEX and arctic air-mass data sets. Quart J R Meteor Soc 112:693–709

Betts AK, Ball JH, Beljaars ACM, Miller MJ, Viterbo P (1994) Coupling between land-surface boundary-layer parametrizations and rainfall on local and regional scales: lessons from the wet summer of 1993. In: Fifth conference on global change studies, Nashville, Tennessee, pp 174–181 (preprint)

Black TL (1994) The new NMC mesoscale Eta model: description and forecast examples. Wea Anal Forecast 9:265–278

Bonatti JP (1996) Modelo de Circulação Geral Atmosférico do CPTEC. Climanálise. Special Edition. INPE. São José dos Campos

Brubaker KL, Entekhabi D (1996) Analysis of feedback mechanisms in land-atmosphere interaction. Water Resour Res 32:1343–1358

Bustamante J, Gomes JL, Chou SC, Rozante JR (1999) Evaluation of April 1999 rainfall forecasts over South America using the Eta model. Climanálise (São José dos Campos), Cachoeira Paulista, SP, No. 5

Chang J-T, Wetzel PJ (1991) Effects of spatial variations of soil moisture and vegetation on the evolution of a prestorm environment: a numerical case study. Mon Wea Rev 119: 1368–1390

Cosby BJ, Hornberger GM, Clapp RB, Ginn TR (1984) A statistical exploration of the relationships of soil moisture characteristics to the physical properties of soils. Water Resour Res 20:682–690

Dirmeyer PA, Dolman AJ, Sato N (1999) The pilot phase of the global soil wetness project. Bull Am Meteorol Soc 80:851–878

Dirmeyer PA, Zeng FJ, Ducharne A, Morrill JC, Koster RD (2000) The sensitivity of surface fluxes to soil water content in three land surface schemes. J Hydrometeorol 1:121–134

Ebert EE, McBride JL (2000) Verification of precipitation in weather systems: determination of systematic errors. J Hydrol 239:179–202

Ek MB, Holtslag AAM (2004) Influence of soil moisture on boundary layer cloud development. J Hydrometeorol 5:86–99

Ek MB, Mitchell KE, Lin Y, Rogers E, Grunmann P, Koren V, Gayno G, Tarpley JD (2003) Implementation of Noah land surface model advances in the National Centers for Environmental Prediction operational mesoscale Eta model. J Geophys Res 108(D22): 8851–8866. doi:10.1029/2002JD003296

Entekhabi D, Brubaker KL (1995) An analytic approach to modeling land-atmosphere interaction. Water Resour Res 31:619–644

Entekhabi D, Rodriguez-Iturbe I, Castelli F (1996) Mutual interaction of soil moisture state and atmospheric processes. J Hydrol 184:3–18

FAO (2007) Digital soil map of the World http://www.fao.org/geonetwork/srv/en/metadata.show?id=14116

Fast JD, McCorcle MD (1991) The effect of heterogeneous soil moisture on a summer baroclinic circulation in the Central United States. Mon Wea Rev 119:2140–2167

Fels SB, Schwarzkopf MD (1975) The simplified exchange approximation. A new method for radiative transfer calculations. J Atmos Sci 32:1475–1488

Findell KL, Eltahir EA (2003a) Atmospheric controls on soil moisture–boundary layer interactions: three-dimensional wind effects. J Geophys Res 108:8385. doi:10.1029/2001JD001515

Findell KL, Eltahir EA (2003b) Atmospheric controls on soil moisture–boundary layer interactions. Part I: framework development. J Hydrometeorol 4:552–569

Grams JS, Gallus WA, Koch SE, Wharton LS, Loughe A, Ebert EE (2006) The use of a modified Ebert-McBride technique to evaluate mesoscale model QPF as a function of convective system morphology during IHOP 2002. Wea Forecast 21:288–306

Gallus WA Jr, Segal M (2000) Sensitivity of forecast rainfall in a Texas convective system to soil moisture and convective parameterization. Wea Forecast 15:509–525

Jackson TJ, Vine DML, Swift CT, Schmugge TJ, Schiebe FR (1995) Large area mapping of soil moisture using the ESTAR passive microwave radiometer in Washita'92. Remote Sens Environ 52:27–37

Jackson TJ, Vine DML, Hsu AY, Oldak A, Starks PJ, Swift CT, Isham JD, Haken M (1999) Soil moisture mapping at regional scales using microwave radiometery: the southern Great Plains hydrology experiment. IEEE Trans Geosci Remote Sens 37:2136–2151

Janjic ZI (1994) The step-mountain eta coordinate model: further developments of the convection, viscous sublayer and turbulence closure schemes. Mon Wea Rev 122:927–945

Kim CP, Entekhabi D (1998) Analysis of feedback mechanisms in the uncoupled and coupled land surface and mixed layer energy budgets. Bound Layer Meteorol 88:1–21

Koch SE, Aksakal A, McQueen JT (1997) The influence of mesoscale humidity and evapotranspiration field in model forecast of cold-frontal squall line. Mon Wea Rev 125:384–409

Koster RD, Dirmeyer PA, Guo Z, Bonan G, Chan E, Cox P, Gordon CT, Kanae S, Kowalczyk E, Lawrence D, Liu P, Lu C-H, Malyshev S, McAvaney B, Mitchell K, Mocko D, Oki T, Oleson K, Pitman A, Sud YC, Taylor CM, Verseghy D, Vasic R, Xue Y, Yamada T (2004) Regions of strong coupling between soil moisture and precipitation. Science 305(5687):1138–1140. doi: 10.1126/science.1100217

Koster RD, Zhichang G, Rongqian Y, Dirmeyer PA, Mitchell K, Puma MJ (2009) On the nature of soil moisture in land surface models. J Clim 22:4322–4335. doi:10.1175/2009JCLI2832.1

Lacis AA, Hansen JE (1974) A parameterization for the absorption of solar radiation in the Earth's atmosphere. J Atmos Sci 31:118–133

Lanicci JM, Carlson TN, Warner TT (1987) Sensitivity of the Great Plains severe-storm environment to soil-moisture distribution. Mon Wea Rev 115:2660–2673

Lau K-M, Bua WR (1998) Mechanisms of monsoon–southern oscillation coupling: insights from GCM experiments. Clim Dyn 14:759–779

Liston GE, Sud YC, Walker GK (1993) Design of a global soil moisture initialization procedure for the simple biosphere model. NASA Tech. Memo. 104590, 130 pp

Mesinger F (1984) A blocking technique for representation of mountains in atmospheric models. Riv Meteorol Aeronaut 44:195–202

Mesinger F, Janjic ZI, Nickovic S, Gavrilov D, Deaven DG (1988) The step-mountain coordinate: model description and performance for cases of Alpine lee cyclogenesis and for a case of Appalachian redevelopment. Mon Wea Rev 116:1493–1518

Mintz Y, Serafini YV (1992) A global monthly climatology of soil moisture and water balance. Clim Dyn 8:13–27

Pielke RA Sr (2001) Influence of the spatial distribution of vegetation and soils on the prediction of cumulus convective rainfall. Rev Geophys 39:151–171

Qu W, Henderson-Sellers A, Pitman AJ, Chen TH, Abramopoulos F, Boone A, Chang S, Chen F, Dai Y, Dickinson RE, Dumenil L, Ek M, Gedney N, Gusev YM, Kim J, Koster R, Kowalczyk EA, Lean J, Lettenmaier D, Liang X, Mahfouf J-F, Mengelkamp H-T, Mitchell K, Nasonova ON, Noilhan J, Robock A, Rosenzweig C, Schaake J, Schlosser CA, Schulz J-P, Shmakin AB, Verseghy DL, Wetzel P, Wood EF, Yang Z-L, Zeng Q (1998) Sensitivity of latent heat flux from PILPS land-surface schemes to perturbations of surface air temperature. J Atmos Sci 55:1909–1927

Reen BP, Stauffer DR, Davis KJ, Desai AR (2006) A case study on the effects of heterogeneous soil moisture on mesoscale boundary-layer structure in the Southern Great Plains, U.S.A. Part II: mesoscale modelling. Bound Layer Meteorol 120:275–314

Riehl H, Badner J, Hovden JE, Laseur NE, Means LL, Palmer WC, Schroeder MJ, Snellman LW (1952) Forecasting in middle latitudes. Am Meteorol Soc Meteorol Monogr 1(5):1–80

Robock A, Vinnikov KY, Srinivasan G, Entin JK, Hollinger SE, Speranskaya NA, Liu S, Namkhai A (2000) The global soil moisture data bank. Bull Am Meteorol Soc 81:1281–1299

Rozante JR, Moreira DS et al (2010) Combining TRMM and surface observations of precipitation: technique and validation over South America. Wea Forecast 25(3):885–894

Santanello JA Jr, Friedl MA, Ek MB (2007) Convective planetary boundary layer interactions with the land surface at diurnal time scales: diagnostics and feedbacks. J Hydrometeorol 8:1082–1097

Schär C, Lüthi D, Beyerle U, Heise E (1999) The soil-precipitation feedback: a process study with a regional climate model. J Clim 12:722–741

Schemm J, Schubert S, Terry K, Bloom S (1992) Estimates of monthly mean soil moisture for 1979–1989. NASA Tech. Memo. 104571, 260 pp

Segal M, Physick WL, Heim J, Arritt RW (1993) On the enhancement of cold front temperature contrasts by differential cloud cover. Mon Wea Rev 121:867–873

Seluchi ME, Chou SC (2001) Evaluation of two Eta model versions for weather forecast over South America. Geofísica Internacional, Mexico 40:219–237

Sutton CJ, Hamill TM, Warner TT (2006) Will perturbing soil moisture improve warm-season ensemble forecasts? A proof of concept. Mon Wea Rev 134:3174–3189

Tomasella J, Hodnett MG (2005) Pedrotransfer functions for tropical soils. In: Pachepsky Y, Rawls WJ (Org.) Developments in soil science: pedotransfer functions in hydrology, vol 30. Elsevier, Amsterdam, pp 415–435

Wilson MF, Henderson-Sellers A, Dickinson RE, Kennedy PJ (1987) Sensitivity of the biosphere-atmosphere transfer scheme (BATS) to the inclusion of variable soil characteristics. J Clim Appl Meteorol 26:341–362

Yang S, Yoo S-H, Yang R, Mitchell KE, van den Dool H, Higgins RW (2007) Response of seasonal simulations of a regional climate model to high-frequency variability of soil moisture during the summers of 1988 and 1993. J Hydrometeorol 8:738–757

Zhu J, Liang X-Z (2005) Regional climate model simulation of U.S. soil temperature and moisture during 1982–2002. J Geophys Res 110:D24110. doi:10.1029/2005JD006472

Zobler L (1986) A world soil file for global climate modeling. NASA Tech. Memo. 87802, 33 pp